Acta Mech
https://doi.org/10.1007/s00707-025-04351-4

ORIGINAL PAPER

P. A. Magalhães · A. L. Araújo · J. F. A. Madeira

Multimodal optimization of piezoelectric patches number and placement for effective structural vibration reduction

Received: 29 November 2024 / Revised: 27 March 2025 / Accepted: 15 April 2025

Abstract The presence of vibrations is a common phenomenon in many applications, with the potential to lead to structural issues. Therefore, control is crucial for reducing oscillation amplitudes, suppressing undesirable resonances, and preventing structural fatigue failures. In this context, the use of piezoelectric patches to act as controllers on plates has been implemented. However, an optimization challenge in this scenario precedes the dynamic study, which is the investigation of patch positioning. In this paper, we developed a model in ANSYS to optimize positioning conditions with the Global and Local Optimization using Direct Search (GLODS) and the Direct Multisearch (DMS) algorithms. The aim is to determine the optimal patch location based on the electromechanical coupling coefficient (EMCC), with GLODS optimizing individual modes and DMS optimizing multiple modes simultaneously. This approach enables the calculation of tuning values for resistances and inductances, effectively mitigating vibration issues.

1 Introduction

Piezoelectric materials have captured the interest of research groups and industrial sectors alike, offering promising avenues for adaptive structures across various applications [1]. Often utilized as thin layers or patches affixed to flexible plate-like structures, these materials form complex composite systems. However, the adoption of multi-layered structures introduces challenges such as structural instability and excessive vibration amplitudes, which can significantly impact material performance and even lead to catastrophic failures [2]. To address these issues, leveraging piezoelectric materials for vibration control is imperative. This necessitates a nuanced approach, including considerations such as optimal patch placement on plate-like structures to unlock their full potential in mitigating vibrations.

The vibration control of intelligent structures can be applied as passive, active or hybrid controls. Passive control involves applying electrical components, such as resistors and inductors, to dissipate energy [3,4]. Active control, on the other hand, involves implementing a feedback control system that acts as a counter-

A. L. Araújo and J. F. A. Madeira contributed equally to this work.

P. A. Magalhães (✉)· A. L. Araújo · J. F. A. Madeira
IDMEC - Instituto de Engenharia Mecânica, Instituto Superior Técnico, Universidade de Lisboa, Av. Rovisco Pais, Lisbon 1049-001, Portugal
E-mail: pedro.p.magalhaes@tecnico.ulisboa.pt

A. L. Araújo
E-mail: aurelio.araujo@tecnico.ulisboa.pt ·

J. F. A. Madeira
ADM, ISEL, Instituto Politécnico de Lisboa, Rua Conselheiro Emídio Navarro 1, Lisbon 1959-007, Portugal
E-mail: aguilarmadeira@tecnico.ulisboa.pt

Published online: 27 May 2025

resonant force [3,5]. Finally, hybrid control combines both feedback mechanisms and electrical dissipation elements in way of mitigate the vibration energy [6–9].

The initial implementation of passive control using piezoelectric materials connected to resistors and inductors was first explored and demonstrated by Forward in [3], where it was shown how these electrical components could alter the structural response. In this way, calibration methods for RL series shunt circuits were introduced by Hagood and Von Flotow [4]. Subsequently, Wu [10] expanded on this by developing calibration techniques for the RL parallel shunt configuration. Since then, numerous other calibration methods have been developed, including approaches involving residual mode correction, as introduced by [11,12], and those considering the effective electromechanical coupling coefficient, as presented in [13,14].

Modeling the resulting electromechanical coupled systems, composed of a flexible plate-like structure with an arbitrary discrete distribution of surface-bonded piezoelectric patches, poses significant challenges. This complexity arises from geometrical and material discontinuities, as well as localized electromechanical coupling phenomena. Due to the complexity of the problem, analytical solutions are only available for a few specific and idealized cases. Therefore, the finite element method (FEM) stands out as the most employed technique for modeling piezoelectric structures. Its capability to handle multi-physics problems and adaptability to address geometric and mechanical discontinuities make it a preferred choice in such scenarios.

Consequently, the optimal placement of a patch necessitates the calculation of the impact of piezoelectric actuation on plate behavior. This impact is quantified through the parameter known as the EMCC, which plays a pivotal role in the tuning of an electromechanical absorber. It is of crucial importance to accurately represent and to maximize this value in order to achieve effective tuning, as evidenced by [15]. The EMCC plays a pivotal role in numerous applications, including passive shunt damping [10,16], improvement of active control authority, piezoelectric power harvesting [17,18], and damage detection [19]. Therefore, optimizing patch placement is essential for maximizing this parameter. By strategically placing the patches, the effectiveness of the control technique's actuation can be significantly enhanced.

In the current context, numerous studies have explored the optimal placement of patches, particularly in relation to beams. Notable examples include [15,20], where the optimal positioning is identified based on beam structures. Additionally, recent papers have addressed patch placement optimization on plates, considering specific optimization parameters for complex surfaces with a single patch [21] as well as with varying numbers of patches [22,23]. However, this paper differs from the existing literature by providing a comprehensive analysis of the impact of patch positioning on plates, maintaining a constant total patch density while varying both position and quantity. This approach allows for greater flexibility and breadth of study, facilitated by the developed FEM approach. In addition, the study highlights the relevance of the EMCC parameter and its importance in vibration attenuation, thereby contributing significantly to advancing research in this field. The primary objective of this study is to offer an in-depth exploration of the problem, with a particular emphasis on the EMCC parameter and the electrical configuration of the patches. Furthermore, the objective is to provide an in-depth analysis of the ANSYS [24] implementation, talking about its functionality, key variables, and validating it through recent publications. Subsequently, the discussion will focus on the patch placement problem, detailing the application of the optimization program GLODS [25] and DMS [26], for single-objective and simultaneous multi-objective conflicts, respectively, these programs are already validated and present in several articles on literature, such as [22,23,27]. These efforts will enable the derivation of results and the drawing of conclusions pertaining to various configurations and modes of vibration within the scope of the problem addressed in this paper.

Thus, after determining the optimal position with the maximum EMCC value, it becomes possible to calculate the resistance and inductance values. As demonstrated in [13], for most practical problems, the tuning formulas depend solely on the two natural frequencies from the short-circuit (SC) and open-circuit (OC) limits and a modal charge that acts as an additional reaction force associated with SC electrodes, as shown in [14] when calculating the resistance and inductance values.

Therefore, the main goal of this article is to initially determine the optimal positions, subsequently ascertain the values of resistances and inductances through the calibration method detailed in [14], and finally, evaluate the outcomes by applying them to the 10 first modes excited individually and modes excited simultaneously, both involving the cases with 1, 4 and 9 patches, maintaining a constant total patch density.

2 Electromechanical coupling

Piezoelectric materials possess the characteristic of converting mechanical energy into electrical energy, and vice versa. When a piezoelectric material deforms, it generates an electric potential, or when a specific electric

potential is applied to the material, it induces deformation [4]. Therefore, piezoelectric materials are described by equations that relate strain, stress, and electric field. These equations can be written as follows:

$$\begin{aligned} \boldsymbol{\epsilon} &= \mathbf{S}^E \boldsymbol{\sigma} + \mathbf{d}^T \mathbf{E}_f \\ \mathbf{D} &= \mathbf{d}\boldsymbol{\sigma} + \boldsymbol{\epsilon}^\sigma \mathbf{E}_f \end{aligned} \tag{1}$$

where $\boldsymbol{\sigma}$ is the mechanical stress vector, $\boldsymbol{\epsilon}$ is the mechanical strain vector, $\mathbf{D}$ is the electric displacement vector, $\mathbf{E}_f$ is the electric field vector, $\mathbf{S}^E$ is the compliance matrix, $\mathbf{d}$ is the piezoelectric coupling matrix in strain form and $\boldsymbol{\epsilon}^\sigma$ is the dielectric matrix measured at constant stress.

As mentioned earlier, due to the complexity of the problem, it is typically addressed using the finite element method. Therefore, it is crucial to formulate the equations representing the equilibrium equations for free vibrations, accounting for the piezoelectric effect. These equations can be presented below:

$$\left[\begin{bmatrix} \mathbf{K_{uu}} & \mathbf{K_{u\phi}} \\ \mathbf{K_{u\phi}}^T & \mathbf{K_{\phi\phi}} \end{bmatrix} - \omega^2 \begin{bmatrix} \mathbf{M} & \mathbf{0} \\ \mathbf{0} & \mathbf{0} \end{bmatrix}\right] \begin{Bmatrix} \mathbf{u} \\ \boldsymbol{\phi} \end{Bmatrix} = \begin{Bmatrix} \mathbf{0} \\ \mathbf{Q} \end{Bmatrix} \tag{2}$$

where $\mathbf{K_{uu}}$, $\mathbf{K_{u\phi}}$ and $\mathbf{K_{\phi\phi}}$ are the stiffness matrices associated with the mechanical displacements, electromechanical coupling and electric potentials, respectively, $\mathbf{M}$ contains the physical mass associated with the inertia of the plate and piezoelectric patches, $\mathbf{Q}$ is the applied electric charges vector, ω is the circular frequency, $\mathbf{u}$ is the vector of mechanical degrees of freedom and $\boldsymbol{\phi}$ is the vector of electric potentials.

In order to achieve this, as demonstrated in equation (2), it is important to comprehend the interconnection between the mechanical and electrical systems. Consequently, it is significant to ascertain the presence and impact of this interconnection within the system. With this approach in mind, the EMCC was determined. According to [15], there are multiple methods to calculate this coefficient. Nevertheless, in this article, the finite element method was employed, allowing for an accurate calculation using the following equation, which avoids approximations. The coefficient can thus be calculated as follows:

$$k^2_{e(m)} = \frac{\omega^2_{OC(m)} - \omega^2_{SC(m)}}{\omega^2_{SC(m)}} \tag{3}$$

where $\omega_{OC(m)}$ represents the natural frequency of the m-th mode when the patches are in an open circuit condition, denoted by electric impedance $Z = \infty$, indicating that the electric charge $\mathbf{Q}$ is equal to zero in eq. (2). Similarly, $\omega_{SC(m)}$ denotes the natural frequency of the m-th mode when the patches are in a short circuit condition, indicated by $Z = 0$, meaning that $\mathbf{Q}$ is not null in eq. (2). These frequencies are derived through finite element analysis of equation (2). It is important to note that the value of $k^2_{e(m)}$ is typically expressed as a percentage.

In this article, the electromechanical coupling coefficient is the primary variable of interest, as it will be used to evaluate each patch position. By analyzing the results, the optimal position for each patch can be determined. For example, in the first mode of vibration, it is expected that the highest $k^2_{e(1)}$ value will be obtained with the patches in the middle of the plate due to the nature of the vibration. This approach enables the identification of the optimal patch configuration.

In this article, the electrical configuration is defined by three main characteristics: Same Polled and Parallel Wire (SP-PW), Parallel Shunt Circuit, and Single Shunt Configuration. The first characteristic describes how the equipotential surfaces of the piezoelectric pairs of patches are connected, the second defines how the electrical components are arranged, and the third specifies how the pairs are interconnected. In order to illustrate each of these characteristics, figure 1 provides a general example of each, respectively, where Z represents the electrical impedance of the circuit.

Accordingly, with the optimal $k^2_{e(m)}$ value, the inductance (L) and resistance (R) values were calculated, as these are responsible for damping vibrations in the studied mode. So, implementing the single shunt configuration, all the patches are connected in a single resistance and inductance, and these electrical elements are placed in parallel distribution. It is crucial to emphasize that in a configuration comprising a single shunt and multiple pairs of patches, the interconnection between the patches must be designed with consideration for modal charge and in accordance with the principles outlined in [14]. The tuning procedure and expressions for resistance and inductance, according to [14], are presented bellow.

$$R_P = \frac{k^2_{e(m)}\,\omega_{SC}}{Q^2_{SC(m)}} \sqrt{\frac{1}{2k^2_{e(m)}}} \tag{4}$$

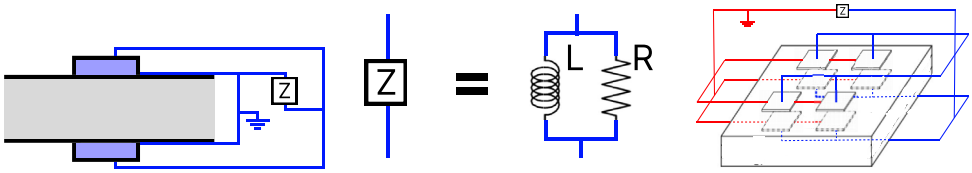

(a) SP-PW configuration. (b) Parallel shunt circuit. (c) Single shunt connection.

Fig. 1 Main characteristics of the electrical configuration circuit

$$L_P = \frac{k^2_{e(m)}}{Q^2_{SC(m)}} \tag{5}$$

where $Q_{SC(m)}$ and $\omega_{SC(m)}$ are, respectively, the modal charge and the natural frequency, in short circuit, calculated by equation (2) for the m-mode.

3 Patch distribution

Given that this work involves numerical implementation with a certain level of automation, and that the primary variable affecting the EMCC value is the position of each patch, it is crucial for the ANSYS program to automate the distribution of patches regardless of their position and quantity. For this purpose, it was considered that the patches could be applied in any position, provided they maintain a grid format, meaning all patches should be distributed in rows and columns. Accordingly, the following distribution intervals were defined for each patch:

$$\begin{aligned}
x_n &\in \left[-\frac{L}{2} + \frac{l}{2} + l_{\text{sizemin}} + \left(n_{patches_x} - n\right)\left(l + l_{\text{sizemin}}\right) \; ; x_{n-1} - l - l_{\text{sizemin}} \right] \\
y_m &\in \left[-\frac{H}{2} + \frac{h}{2} + l_{\text{sizemin}} + \left(n_{patches_y} - m\right)\left(h + l_{\text{sizemin}}\right) \; ; \; y_{m-1} - l - l_{\text{sizemin}} \right] \\
n &= 1, 2, ..., n_{patches_x} \\
m &= 1, 2, ..., n_{patches_y}
\end{aligned} \tag{6}$$

where $n_{patches_x}$ represents the quantity of patches in the x-direction or the number of columns, $n_{patches_y}$ represents the quantity of patches in the y-direction or the number of rows, l denotes the length of the patch, h denotes the height of the patch, L represents the length of the plate, H represents the height of the plate, and $l_{sizemin}$ represents the length of the mesh element. Furthermore, for equation (6), consider $x_0 = \frac{L}{2} + \frac{l}{2}$ and $y_0 = \frac{H}{2} + \frac{h}{2}$.

4 Numerical implementation

The electromechanical structure was modeled in ANSYS. It is first necessary to note that this code was developed in order to ensure its generality, allowing it to be implemented in various scenarios. Thus, based on the steps outlined by [14] and summarized in the flowchart showed in Figs. 2 and 3, the following steps are presented to offer a succinct explanation of the implementation:

1. **Input parameters**
   The input parameters of the model are related to the number of patches, divided into the quantity present along the X-axis and the quantity present along the Y-axis. It is worth noting that the model was constructed in such a way that the patches can only be divided into rectangular shapes, i.e., in rows and columns. Another input parameter is the geometry of the patches and plate, assuming that all patches have the same dimensions. Additionally, there are parameters related to material and electrical properties. Another crucial parameter, particularly in the context of this article, is the patch position parameter. This variable is passed to the program through a file named "Input_GeometricParameters", which is a text file containing one value of the X-coordinate on each line. Once all X-coordinates have been defined, all the Y-coordinates must be represented. Lastly, input parameters related to mesh, boundary conditions, and analyses are presented.

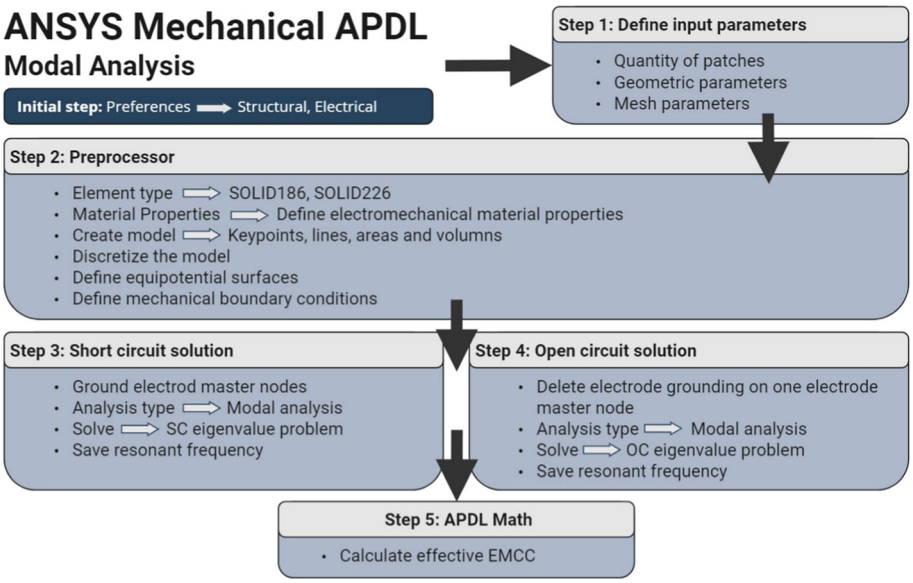

Fig. 2 Flowchart illustrating modal analysis in ANSYS

2. **Preprocessor**
   Initially, one must select "Structural" and "Electrical" analyses. This is followed by defining the geometry, material properties, element types, and mesh partitions of the analyzed electromechanical structure. In this study, SOLID186 and SOLID226 3D elements are employed for discretizing the host structure and piezoelectric patch(es), respectively. Subsequently, boundary conditions and equipotential (EP) conditions are imposed on all continuous electrodes within the discretized model. For each continuous electrode, the EP condition is defined at a master node, which is saved for future reference.
3. **OC solution**
   In this stage, it is essential to note that the electrical circuit between the external and internal surfaces of the patches is not connected. In other words, it implies that the electrical inductance is very high, consequently preventing the flow of electric current. To represent this in the ANSYS model, simply remove the connections between these surfaces. The objective of this stage is to calculate the resonance frequency (ω_r) for each desired mode.
4. **SC solution**
   In this step, a zero electric potential is applied to the master nodes to configure the piezoelectric patch(es) as a short circuit (SC). Subsequently, a modal analysis is conducted to ascertain the targeted SC resonant frequency (ω_r) and modal charge (Q_r), the latter representing the "reaction force" of the modal analysis.
5. **APDL Math**
   Finally, it essentially requires calculating the values of k_e^2 (EMCC) using the equation defined previously by eq. (3).

By following the previously outlined steps, it becomes possible to obtain results for models with various imposed conditions. This approach renders the model more generic and comprehensive, thus making it suitable for addressing the problem at hand.

In addition to modal analysis, this project also encompasses harmonic analysis, which can be seen in Fig. 3. This phase is crucial because it permits the observation of how the resistance and inductance affect the resonance peak. In ANSYS, the harmonic analysis is performed according to the steps outlined in Fig. 2, with modifications for step 2 and beyond. In particular, electrical components, such as resistance and inductance, are introduced and an electric circuit is applied between the plates. In the present study, a single shunt circuit was assumed.

In a single shunt circuit, all patches are connected, resulting in a single value for both resistance and inductance. It is crucial to emphasize that in this type of circuit, the modal charges of the patches exert a significant influence on the connections between them. In the typical case where all patches have positive modal charges, the outer surfaces of the patches are connected together, and the inner surfaces are connected in a similar manner. However, if any patch exhibits a negative modal charge, the connection strategy is altered.

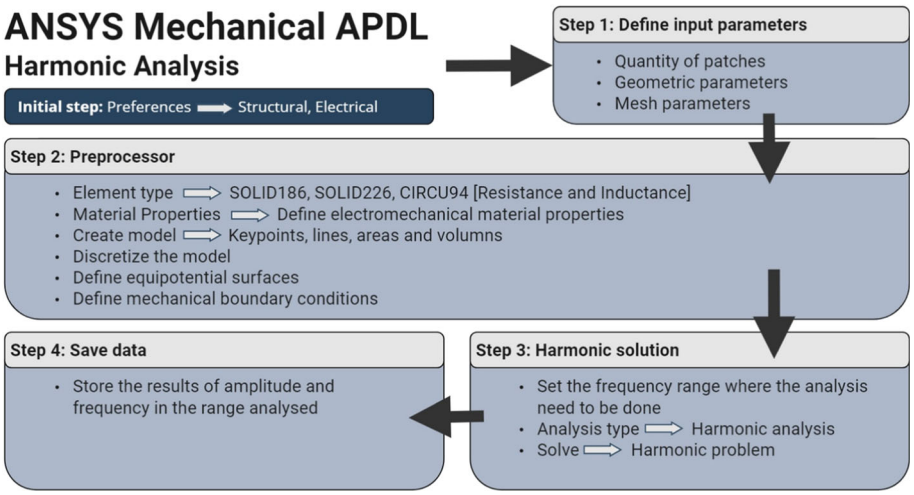

Fig. 3 Flowchart illustrating harmonic analysis in ANSYS

Table 1 Dimensions of each patch in each case

Pairs of patches	l [m]	w [m]	Thickness [m]
1	0.0828	0.0628	0.0005
4	0.0414	0.0314	0.0005
9	0.0276	0.0209	0.0005

In such cases, the patch with the negative modal charge requires alternating connections: its inner surface is connected to the outer surfaces of the other patches, and its outer surface is connected to the inner surfaces of the other patches.

The third step of this analysis is to solve the harmonic problem for a specific frequency range. And finally, the final step is to store the values of the amplitude behavior in frequency and analysis the peak of resonance.

A crucial aspect of this analysis is the selection of the force application and analysis points. In this study, the selection was based on the modal configuration of the plate for each mode, focusing on areas of maximum deformation, highlighted in red in the displacement color chart.

For single-objective cases, the selection is straightforward since only one mode is excited, and the force and analysis points can both be placed at the maximum deformation region. However, for multi-objective cases, the process is more complex, once regions with high deformation for one mode may have little deformation for another. To address this, as in the multi-mode analyses, a frequency range covering 3 modes was chosen, three force application points were selected, each corresponding to the maximum deformation of each of the three modes studied. The analysis point was chosen at an intermediate position relative to these three points to capture the deformation behavior across the frequency range.

About the dimensions, a plate with dimensions of 0.414 m in length, 0.314 m in width, and 0.001 m in thickness were fixed, and the value of l_{sizemin} equal to $5.175 \cdot 10^{-3}$ [m]. For the patches, it was assumed that all patches have the same dimensions when their number is fixed. Therefore, altering the number of patches changes their length and width such that the total surface area of the patches remains constant. However, in both cases the thickness is fixed at 0.0005 m. The individual patch dimensions for each case are presented in Table 1.

In addition, the material of the plate is aluminum, with elastic properties $E = 70$ GPa, $\nu = 0.33$ and specific mass $\rho = 2700\ kg/m^3$. Lead zirconate titanium (PZT-5H) is the material used for the piezoelectric patches, its properties were taken from [28] and are presented in Table 2.

Where $\epsilon_R = \frac{\epsilon^\sigma}{\epsilon_0}$ is the relative permittivity and the reference value is the absolute dielectric permittivity of vacuum, $\epsilon_0 = 8.854 \cdot 10^{-12}$ F/m.

Table 2 Material properties for PZT-5H [28]

S^E [$\times 10^{12}$ Pa^{-1}]	d [$\times 10^{-12}$ C/N]	ϵ_R	ρ [kg/m^3]
$S_{11}^E = 16.5$	$d_{31} = -274$	$(\epsilon_R)_{11} = 3130$	7500
$S_{12}^E = -4.78$	$d_{31} = -274$	$(\epsilon_R)_{22} = 3130$	
$S_{13}^E = -8.45$	$d_{33} = 593$	$(\epsilon_R)_{33} = 3400$	
$S_{33}^E = 20.7$	$d_{24} = 741$		
$S_{44}^E = 43.5$	$d_{15} = 741$		
$S_{55}^E = 43.5$			
$S_{66}^E = 42.6$			

5 Optimization

The single-objective optimization algorithm GLODS, as documented in [25], is particularly suited for bound-constrained, derivative-free, and global optimization tasks. Developed with the specific purpose of identifying the largest number of local minima, GLODS employs a search procedure based on direct search of a directional type, ultimately leading to the identification of the global minimum.

In order to achieve this, given the objective of the paper, which is to find the maximum rather than the minimum of the objective function EMCC, a mathematical workaround was required. Since the GLODS optimization program is designed to find the minimum of a function, the solution was to minimize the negative of $k_{e(m)}^2$. Thus, the desired maximum is obtained as the negative of this minimum:

$$max\,(f(x)) = -min\,(-f(x)) \tag{7}$$

where $f(x)$ represents the objective function, which, in this case, corresponds to the value of k_e^2 (EMCC).

It is important to emphasize that the program initialization offers flexibility with various sampling methods. These methods can be a list of points with a single entry, Latin hypercube sampling, random sampling, equally spaced points along a line segment defined by the variable upper and lower bounds, inclusion of the central point, or the option to utilize a custom list provided by the user.

The DMS multi-objective optimization algorithm, as detailed in [26], was incorporated into this study to address the need for a multi-objective approach. As shown in the results section, certain modes, especially those with high frequency, display resonance peaks that occur close together and vary across frequency ranges depending on the number of patches applied to the plate. Given these characteristics, it was essential to adopt a multi-objective method to maximize not just a single EMCC value but all EMCC values for the modes excited within the frequency range under investigation.

The method implemented in the Direct Multisearch (DMS) program is designed to identify the Pareto front in multi-objective optimization problems. The Pareto front represents the set of optimal solutions for the specific problem, comprising all non-dominated points. Each point on this front signifies a solution in which improving any one objective would lead to a deterioration in at least one other objective. Unlike single-objective approaches, the DMS algorithm produces a set of non-dominated solutions, each ensuring that improving one objective inevitably leads to a reduction in at least one other.

5.1 Percentage position approach

For a better implementation of the optimization program, a change in the way position values are read was performed. A percentage-based approach was employed, meaning that the position of the patch is now represented by a percentage value relative to the range within which that patch can be situated, rather than by a real value. This change is extremely relevant for optimization because it allows for the definition of a general range that always varies from 0 to 1. Discretization can now be more easily defined within this range. For example, discretization can be set at intervals of 0.1 within the range of 0 to 1.

In this way, the methodology essentially operates by considering the available intervals for each variable as showed in equation (6), and then transforming this interval into a percentage range. Once the optimization

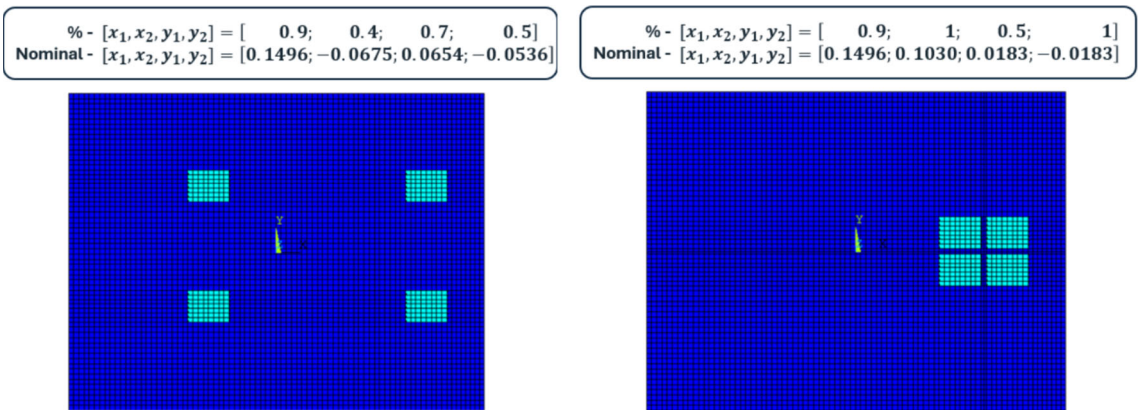

Fig. 4 Relation between percentage and nominal values of position

program runs for the selected percentage value, it converts back to the nominal value, and using this value, the ANSYS program is executed for the given problem. It is worth noting that the optimization program stores the percentage values. Therefore, it is crucial to remember that if testing is required, the necessary conversions must be made, taking into account their respective nominal intervals showed in equation (6).

To illustrate this new approach to position, Figure 4 provides insight into the nominal and percentage values for the proposed distribution problem.

5.2 Uni-objective optimization algorithm

To obtain more accurate results for the optimal patch positions, the optimization process involved increasing the percentage interval of each patch, thereby improving the precision of their placement. Initially, a discretization with a 0.1 percentage interval was applied, followed by optimization with random initialization performed five times. Subsequently, using the same 0.1 interval, initialization was based on the points stored in the cache. To further refine the analysis, the interval was reduced to 0.05, and finally to 0.01, with optimization initialization starting from the best points in the cache. This algorithm allowed for the optimal distribution for each problem.

Therefore, the main challenges revolved around maximizing the value of EMCC, with a detailed analysis conducted for each mode from 1 to 10, separately. In order to achieve this, three single-objective optimization (SOO) problems were formulated:

Problem 1 Simply supported plate with one pair of patches;

$$\begin{aligned} &\text{Minimize} \quad F(\mathbf{x}) = -k^2_{e(\mathrm{a})} \\ &\text{Where} \\ &\qquad \mathbf{x} = [x_1, y_1]^T \\ &\text{Subject to} \\ &\qquad x_n \in [0 : \text{interval} : 1] \\ &\qquad y_m \in [0 : \text{interval} : 1] \\ &\text{For } n = 1 \\ &\text{For } m = 1 \end{aligned} \tag{8}$$

Problem 2 Simply supported plate with four pairs of patches;

$$\begin{aligned} &\text{Minimize} \quad F(\mathbf{x}) = -k^2_{e(\mathrm{a})} \\ &\text{Where} \\ &\qquad \mathbf{x} = [x_1, x_2, y_1, y_2]^T \\ &\text{Subject to} \\ &\qquad x_n \in [0 : \text{interval} : 1] \\ &\qquad y_m \in [0 : \text{interval} : 1] \\ &\text{For } n = 1, 2 \\ &\text{For } m = 1, 2 \end{aligned} \tag{9}$$

Problem 3 Simply supported plate with nine pairs of patches.

$$\begin{aligned}
&\text{Minimize} \quad F(\mathbf{x}) = -k^2_{e(\mathrm{a})} \\
&\text{Where} \\
&\qquad \mathbf{x} = [x_1, x_2, x_3, y_1, y_2, y_3]^T \\
&\text{Subject to} \\
&\qquad x_n \in [0 : \text{interval} : 1] \\
&\qquad y_m \in [0 : \text{interval} : 1] \\
&\text{For } n = 1, 2, 3 \\
&\text{For } m = 1, 2, 3
\end{aligned} \tag{10}$$

5.3 Multi-objective optimization algorithm

Similar to the uni-objective optimization algorithm, this multi-objective algorithm also increased the percentage interval for patch placement. The same intervals were used in both approaches, as they proved effective, and the points studied in the uni-objective approach were reused as storage points in the multi-objective approach. This reuse made the optimization process faster since the objectives values for these points had already been calculated.

To achieve this, the following three multi-objective optimization (MOO) problems were formulated. As can be seen, the problems discussed in Sect. 5.2 are similar to these. The main differences lie in the number of objectives and the fact that, instead of yielding an optimal value, the result is a list of possible optimal points for the analysis.

Problem 1 Simply supported plate with one pair of patches;

$$\begin{aligned}
&\text{Minimize} \quad F(\mathbf{x}) = \left(-k^2_{e(\mathrm{a})}, -k^2_{e(\mathrm{b})}, -k^2_{e(\mathrm{c})}\right) \\
&\text{Where} \\
&\qquad \mathbf{x} = [x_1, y_1]^T \\
&\text{Subject to} \\
&\qquad x_n \in [0 : \text{interval} : 1] \\
&\qquad y_m \in [0 : \text{interval} : 1] \\
&\text{For } n = 1 \\
&\text{For } m = 1
\end{aligned} \tag{11}$$

Problem 2 Simply supported plate with four pairs of patches;

$$\begin{aligned}
&\text{Minimize} \quad F(\mathbf{x}) = \left(-k^2_{e(\mathrm{a})}, -k^2_{e(\mathrm{b})}, -k^2_{e(\mathrm{c})}\right) \\
&\text{Where} \\
&\qquad \mathbf{x} = [x_1, x_2, y_1, y_2]^T \\
&\text{Subject to} \\
&\qquad x_n \in [0 : \text{interval} : 1] \\
&\qquad y_m \in [0 : \text{interval} : 1] \\
&\text{For } n = 1, 2 \\
&\text{For } m = 1, 2
\end{aligned} \tag{12}$$

Problem 3 Simply supported plate with nine pairs of patches.

$$\begin{aligned}
&\text{Minimize} \quad F(\mathbf{x}) = \left(-k^2_{e(\mathrm{a})}, -k^2_{e(\mathrm{b})}, -k^2_{e(\mathrm{c})}\right) \\
&\text{Where} \\
&\qquad \mathbf{x} = [x_1, x_2, x_3, y_1, y_2, y_3]^T \\
&\text{Subject to} \\
&\qquad x_n \in [0 : \text{interval} : 1] \\
&\qquad y_m \in [0 : \text{interval} : 1] \\
&\text{For } n = 1, 2, 3 \\
&\text{For } m = 1, 2, 3
\end{aligned} \tag{13}$$

Table 3 Local minimum computed by GLODS for one pair of patch

Modes	Position		Results					
	x_1	y_1	f_{OC}	f_{SC}	k_e^2	$\frac{Q_{SC}^2}{\omega_{SC}^2}$	L_p	R_p
	%		[Hz]	[Hz]	[%]	[μ (Cs/rad)^2]	[H]	[kΩ]
1	50	50	36.16	35.83	1.89	0.0103	35.42	41.45
2	17	50	79.97	79.11	2.20	0.0119	7.44	17.70
3	50	19	112.62	111.29	2.41	0.0132	3.73	11.91
4	11	21	152.67	150.50	2.91	0.0155	2.09	8.21
5	50	77	157.42	156.60	1.05	-	-	-
6	50	86	227.87	225.00	2.56	0.0142	0.90	5.64
7	37	50	244.31	240.70	3.02	0.0170	0.78	4.78
8	5	50	264.70	261.12	2.76	0.0146	0.70	4.89
9	20	50	286.83	283.81	2.14	0.0112	0.60	5.17
10	35	78	335.85	332.64	1.94	0.0100	0.44	4.71

Table 4 Local minimum computed by GLODS for four pairs of patches

Modes	Position				Results					
	x_1	x_2	y_1	y_2	f_{OC}	f_{SC}	k_e^2	$\frac{Q_{SC}^2}{\omega_{SC}^2}$	L_p	R_p
	[%]				[Hz]	[Hz]	[%]	[μ (Cs/rad)^2]	[H]	[kΩ]
1	51	100	51	100	36.05	35.73	1.77	0.0097	36.97	43.76
2	16	100	51	100	79.34	78.59	1.92	0.0104	7.54	19.01
3	51	100	81	100	111.59	110.43	2.12	0.0116	3.80	12.82
4	10	100	79	100	151.10	149.30	2.43	0.0129	2.13	9.09
5	8	100	58	73	154.92	153.49	1.88	0.0096	2.11	10.50
6	67	100	50	100	240.00	237.03	2.53	0.0140	0.81	5.37
7	56	22	49	100	235.25	232.22	2.63	0.0137	0.90	5.72
8	60	66	51	100	250.10	246.70	2.78	0.0151	0.76	5.02
9	75	32	87	15	269.85	267.13	2.05	0.0111	0.65	5.41
10	92	45	75	33	320.35	316.84	2.23	0.0121	0.47	4.40

6 Results and discussions

This section presents the results of the study related to the three problems previously outlined in Sect. 5, where it is crucial to highlight the significance of employing the percentage position approach outlined in Sect. 5.1. As demonstrated, although the interval remains constant from 0 to 1, the nominal values vary, necessitating calculation using equation (6).

6.1 Modal analyses considering vibration modes individually

Utilizing the GLODS program to solve equations (8), (9) and (10), and implementing the algorithm method in Sect. 5.2, the following optimal positions were found in Tables 3, 4 and 5, respectively.

An important point to note in Table 3 is the low value of k_e^2 (EMCC) when mode 5 is examined. This is because modes 5 and 4 in this problem have very close natural frequencies. Consequently, there will be instances during the optimization where the configurations of these modes will be interchanged, resulting in a lower optimal state compared to other modes. In addition, this low value of k_e^2 results in such a low modal charge, and consequently high values of resistance and inductance that it is not applicable.

As can be observed in the Table 4, the calculated values of inductance and resistance for each mode are comparable to those of the single pair of patches. This is typically due to the fact that when comparing the values of k_e^2, these values are also similar. This suggests that, when the patches are positioned optimally, the number of patches has a minimal impact on the response in the majority of modes. It is important to note that the increase in the number of patches, as discussed in this article, is done while maintaining the total mass of the patches constant.

Table 5 Local minimum computed by GLODS for nine pairs of patches

Modes	Position						Results					
	x_1	x_2	x_3	y_1	y_2	y_3	f_{OC}	f_{SC}	k_e^2	$\frac{Q_{SC}^2}{\omega_{SC}^2}$	L_p	R_p
	[%]						[Hz]	[Hz]	[%]	$[\mu\ (^{Cs}/_{rad})^2]$	[H]	[kΩ]
1	50	100	100	50	100	100	35.98	35.68	1.69	0.0092	36.58	44.63
2	84	100	100	50	100	100	79.07	78.37	1.79	0.0096	7.67	19.95
3	50	100	100	83	100	100	110.95	109.89	1.93	0.0105	3.86	13.56
4	91	100	100	22	100	100	150.38	148.80	2.14	0.0113	2.17	9.80
5	8	99	100	64	76	88	153.97	152.74	1.62	0.0084	2.09	11.15
6	85	48	100	50	100	100	234.19	231.33	2.49	0.0132	0.89	5.83
7	56	100	25	50	100	100	234.46	231.71	2.39	0.0127	0.89	5.93
8	93	100	13	50	100	100	248.95	246.11	2.35	0.0124	0.78	5.61
9	72	28	100	85	67	100	269.71	267.38	1.75	0.0094	0.66	5.90
10	90	76	15	72	28	100	310.83	307.91	1.91	0.0103	0.49	4.90

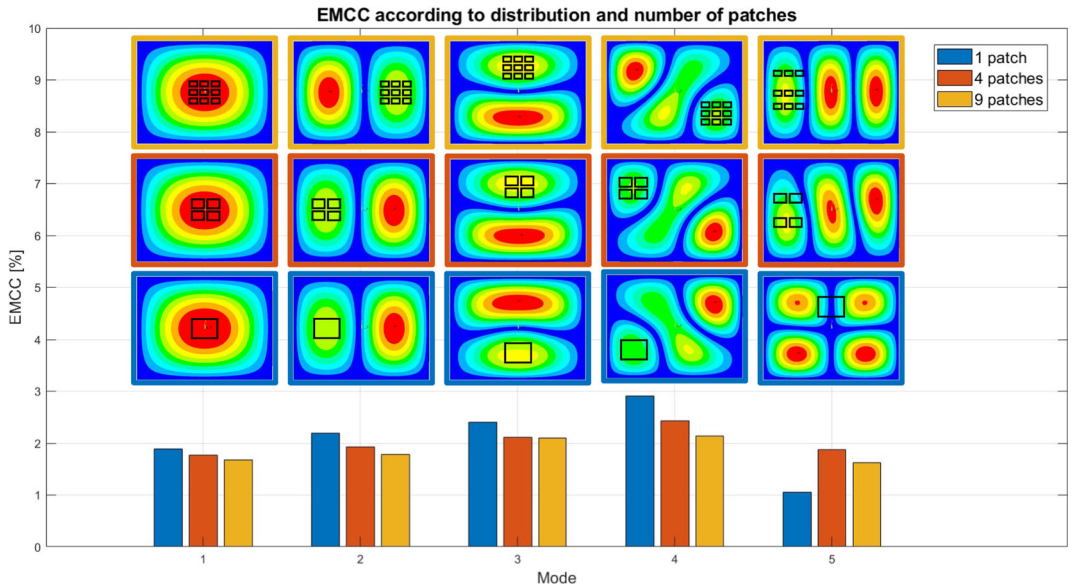

Fig. 5 k_e^2 values and their distribution for each case from modes 1 to 5

As with the preceding problem, the same conclusions can be drawn in this instance. As can be seen, the values of resistances and inductances are all similar when comparing the three problems for each mode. Therefore, the main challenge is to identify the optimal position for the vibration damping problem.

Summarizing the results from Tables 3, 4 and 5, there is a general decrease in the values of k_e^2 (EMCC) as the number of patches increases. This phenomenon occurs because, with the quantity of piezoelectric material maintained at a constant level and the optimal positions often requiring patches to be placed in close proximity to one another, the increase in the number of patches necessitates the maintenance of a minimum distance between them. Consequently, the patches tend to move away from the regions critical for that mode of vibration, thereby reducing the value of k_e^2.

These results are illustrated in Figs. 5 and 6, which presents the maximum k_e^2 values and the absolute displacement of the plate for each mode across optimal configurations of the listed patch quantities in each of the previously addressed issues.

6.2 Sensitivity of the minimum distance between patches

As discussed previously, an increase in the number of pairs of patches can sometimes result in a smaller value of k_e^2 compared to cases with fewer pairs. To investigate this phenomenon, a study was conducted to compare how the minimum distance between patches impacts the value of k_e^2.

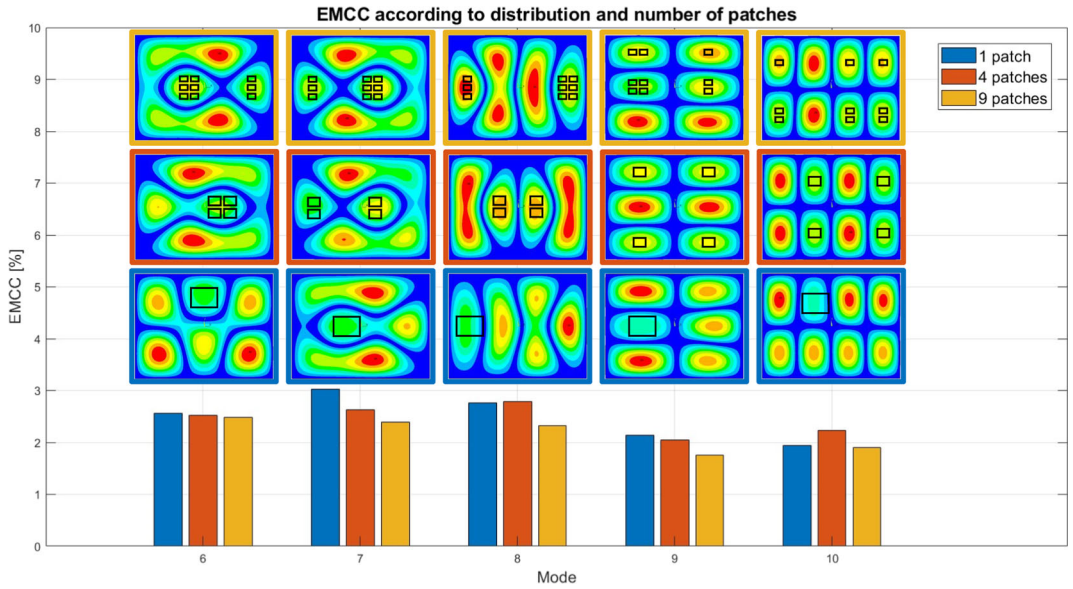

Fig. 6 k_e^2 values and their distribution for each case from modes 6 to 10

Table 6 Values of k_e^2 for different electric connection configurations and minimum distances between pairs of patches

l_{sizemin} [mm]	k_e^2 [%]	
	Same Voltage	Different Voltage
5.175	1.77	1.77
3.881	1.79	1.79
2.588	1.80	1.80

For this sensitivity analysis, the case of 4 pairs of patches and mode 1 was chosen, as it is a favorable mode for study due to its simpler distribution. The study was carried out using two approaches. The first approach involved decreasing the minimum distance between patches. The second approach involved applying the same voltage to all outer surfaces of the patches, which can be conceptualized as having a single pair with parts separated by a certain distance. Therefore, this study will allow to understand what is the main characteristic that impacts the value of k_e^2. The Table 6 shows the results comparing these 2 approaches.

As can be seen in the Table 6, the primary characteristic that impacts the value of EMCC is the minimum distance between pairs of patches. Applying the same voltage to all pairs did not change the value of k_e^2 due to the distribution of them in mode 1, since all pairs of patches are located in the same peak region, the voltage between patches remains the same whether the same or different voltages are applied. Therefore, the value of l_{sizemin} is the most significant factor in this study.

6.3 Harmonic analyses considering vibration modes individually

By applying the respective resistance and inductance values for each mode, as calculated and presented in Tables 3, 4 and 5, the harmonic results were obtained for the first four modes and showed in Fig. 7. The data were presented with a normalized amplitude in order to enhance visualization and facilitate comparison of the results. In all cases, the data were normalized in relation to the maximum value observed in the one-patch scenario. Consequently, the 1 pair of patches curve intersects the x-axis at the value of 1 in all the graphs.

In terms of the results, they are in accordance with expectations. As previously discussed, the optimal positions for each one of the first three modes in the different three problems studied are essentially the same. The only factor that affects the $k_{e(m)}^2$ values is the minimum distance between patches, as concluded in Sect. 6.2. Therefore, for these first four modes, it was expected that the 1-pair configuration would be the most effective in reducing the resonant peak, which is confirmed by the results shown in the Fig. 7.

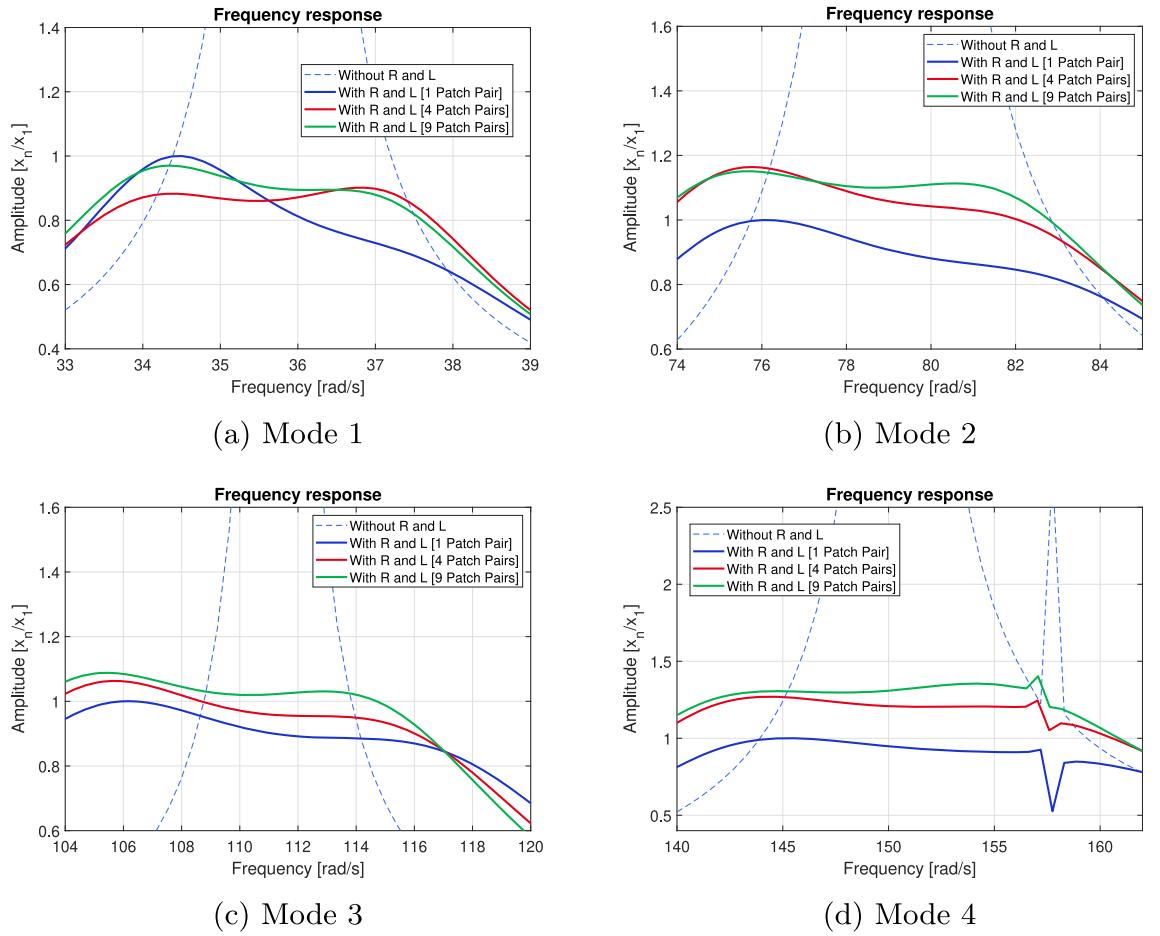

Fig. 7 Frequency response comparing the attenuation of resonant peaks for the first 4 modes when 1, 4 and 9 pairs of patches are applied

It should be noted, however, that this conclusion can only be drawn for these lower modes. As seen in the frequency response of mode 4, presented in Fig. 7d , as the frequency increases, the resonance peaks of each mode move closer to the peaks of the next mode. This phenomenon leads to the discontinuity observed in Fig. 7d , which represents the resonance peak of the next mode-mode 5 in this case.

So, upon analysis of the remaining modes with higher frequencies, as evidenced in Tables 3, 4 and 5, it becomes evident that studying the mode in isolation is not a viable approach. This is due to the fact that these modes are excited in different ranges of frequency, depending on the number of patches involved. Furthermore, it is notable that the frequency range of one mode can overlap with that of another mode in a different configuration of patch numbers. Fig. 8 provides a representation of the varying peak positions when comparing the optimal result of mode 7 for each problem.

Therefore, considering that for higher-frequency modes, the isolation study is not a suitable approach, this paper introduces the analysis of multiple vibration modes, focusing on those with closely spaced resonance peaks. To explore this approach, and based on the frequency values in Tables 3, 4, and 5, the next section applies the optimization strategy considering the modes 6, 7 and 8.

6.4 Modal analyses considering multiple vibration modes

Accordingly, a multi-objective optimization approach was used for the high-frequency modes, as described in Sect. 5.3. In this case, the DMS program was used to solve for modes 6, 7 and 8 simultaneously, resulting in the Pareto front in three dimensions. For further analysis, the Pareto front is also shown for pairs of variables,

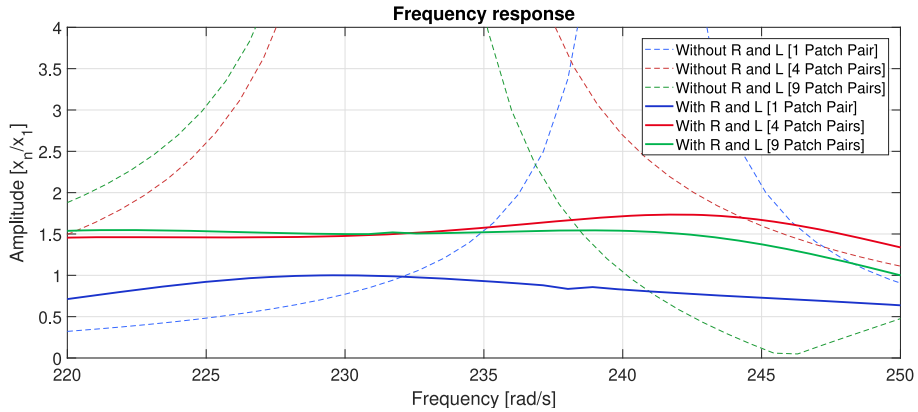

Fig. 8 Harmonic analysis of mode 7 considering different number of pairs of patches

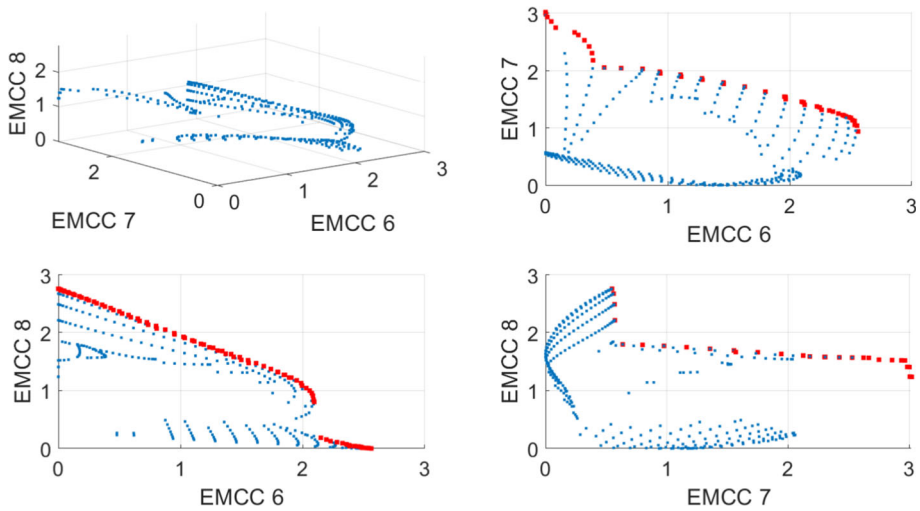

Fig. 9 Pareto front of the 1 pair of patches position in frequency range of modes 6, 7 and 8

specifically for the combinations of modes 6 and 7, 7 and 8, and 6 and 8. As shown in Figs. 9, 10 and 11, the 2D Pareto front for each pair is highlighted in red for clarity.

While no assumptions can be made at this stage, it is important to highlight the flat Pareto front showed in Fig. 9 in the case of EMCC 7 and EMCC 8. This could be either positive or negative, as it indicates that there are many possible optimal points where improving one objective does not significantly impact the other. However, since the study is, actually, with three objectives, it is possible that the optimal solution lies outside of these two objectives. This will be evaluated further in the subsequent analysis.

Based on the previously presented Pareto fronts, the next crucial step is selecting the optimal point from the Pareto front for the problem at hand. This selection was approached using two distinct methods: Minimum Euclidean Distance and Maximum Harmonic Average.

The selection of these metrics for analysis and validation within the multi-objective approach was based on their ability to maximize all $k^2_{e(m)}$ values across the various modes studied. Different metric scenarios were tested, and these specific choices were selected as they ensured consistently high $k^2_{e(m)}$ values without prioritizing one mode over another. Methods such as the Max-Min and Min-Max approaches were considered; however, their optimal results were lower than those obtained with the selected method.

For instance, in the configuration with four patch pairs, the following results were obtained for each method:

As shown in Table 7, although the Min-Max and Max-Min methods yield more uniform results, they tend to excessively weight uniform values of $k^2_{e(m)}$. In contrast, the selected method, while exhibiting slightly lower $k^2_{e(m)}$ values in certain modes, achieves higher values overall without compromising the performance of the

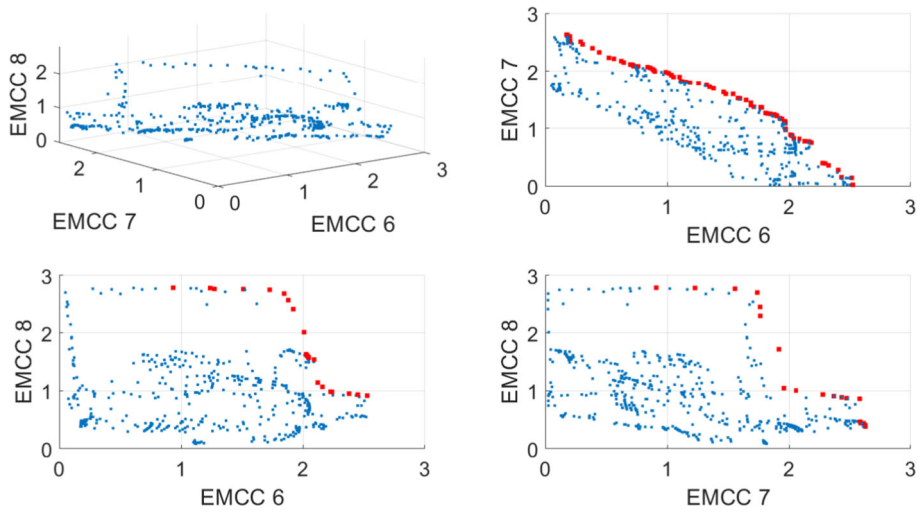

Fig. 10 Pareto front of the 4 pairs of patches position in frequency range of modes 6, 7 and 8

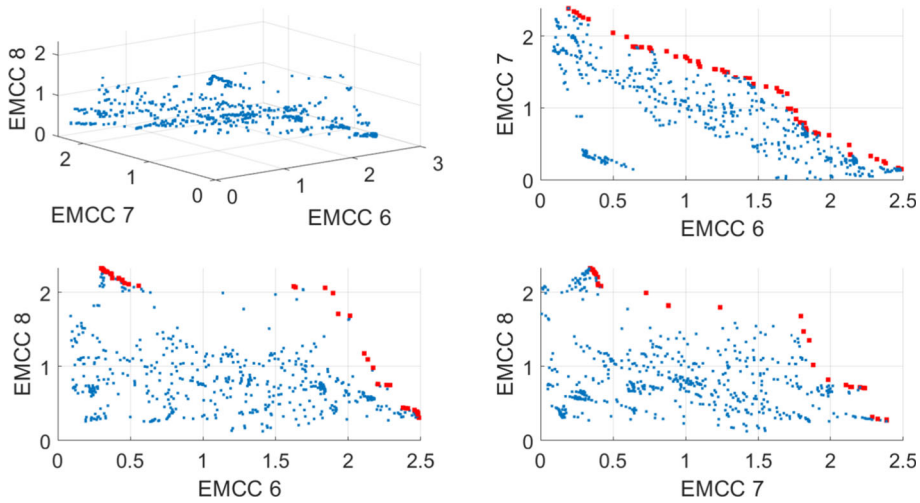

Fig. 11 Pareto front of the 9 pairs of patches position in frequency range of modes 6, 7 and 8

Table 7 Comparison of $k^2_{e(m)}$ values for different methods in the four patch pair configuration

Method	$k^2_{e(6)}$	$k^2_{e(7)}$	$k^2_{e(8)}$
Harmonic Average	0.9346	0.9100	2.7827
Minimum Euclidean Distance	1.4347	1.1942	0.9516
Min-Max Method	1.1361	1.0607	1.1075
Max-Min Method	1.0416	1.1202	1.0916

remaining modes. Therefore, the selected metrics provide a more balanced and effective approach for this study.

- Minimum Euclidean Distance
  This method identifies the point on the Pareto front that is closest to the average of all points, ensuring that all objectives are, at minimum, as close as possible to their respective average values without significantly

Table 8 Local minimum computed by Minimum Euclidean Distance for each number of pairs of patches

Pairs of patches	Position Values						Electrical Values		k_e^2
	x_1 [%]	x_2	x_3	y_1	y_2	y_3	L_p [H]	R_p [kΩ]	[%]
1	31	–	–	47	–	–	0.79	5.10	[1.3048 1.2508 1.3190]
4	35	100	–	51	100	–	0.82	5.37	[1.4347 1.1942 0.9516]
9	88	80	100	72	27	100	0.85	5.81	[1.1783 0.9604 0.8537]

disadvantaging any objective. Mathematically, the process can be expressed as follows:

$$\begin{aligned}
\mu_6 &= \frac{1}{N}\sum_{j=1}^{N} k^2_{e,j(6)} \\
\mu_7 &= \frac{1}{N}\sum_{j=1}^{N} k^2_{e,j(7)} \\
\mu_8 &= \frac{1}{N}\sum_{j=1}^{N} k^2_{e,j(8)} \\
d_j &= \sqrt{\left(k^2_{e,j(6)} - \mu_6\right)^2 + \left(k^2_{e,j(7)} - \mu_7\right)^2 + \left(k^2_{e,j(8)} - \mu_8\right)^2} \\
\text{for } j &= [1, 2, \cdots, N] \\
x_{\text{optimum}} &= x_k \quad \text{where} \quad d_k = \min\left(d_1, \cdots, d_N\right)
\end{aligned} \tag{14}$$

where the subscript j indicates the j-th point on the Pareto front, $k^2_{e,j(m)}$ represents the Effective EMCC value for the m-th mode at the j-th point, N is the total number of points on the front, and μ_6, μ_7, and μ_8 represent the average values of the respective EMCC objectives. The optimal point x_{optimum} corresponds to the k-th point with the minimum Euclidean distance d_k to the computed averages.

- Maximum Harmonic Average
  This approach balances trade-offs by penalizing extreme discrepancies between objectives, ensuring that no single objective is significantly worse than others. It is a good method when all objectives are of similar importance, as the problem in question, once it encourages consistent performance across all objectives and avoids solutions that optimize one objective at the expense of others. This can be showed in the following equation:

$$\begin{aligned}
H_j &= \left(\frac{1}{k^2_{e,j(6)}} + \frac{1}{k^2_{e,j(7)}} + \frac{1}{k^2_{e,j(8)}}\right)^{-1} \quad \text{for } j \quad = [1, 2, \cdots, N] \\
x_{\text{optimum}} &= x_k \quad \text{where} \quad H_k = \min\left(H_1, \cdots, H_N\right)
\end{aligned} \tag{15}$$

As in equation (14), subscript j represents the j-th point on the Pareto front.

6.5 Harmonic analyses considering multiple vibration modes

Using the previously described methods, Tables 8 and 9 present the optimal positions obtained for each problem. In each case, the values of resistance and inductance were calculated as the average of the values listed in Tables 3, 4, and 5 for modes 6, 7, and 8.

So, the main objective of this analysis is to identify, for each number of patches, which selection method Euclidean Distance or Harmonic Average-yields the lowest vibration peak. Once the best option is identified for each patch configuration, a comparison will be made among these optimal choices. This comparison will enable to conclude which approach proves most effective within the frequency range corresponding to modes 6, 7, and 8.

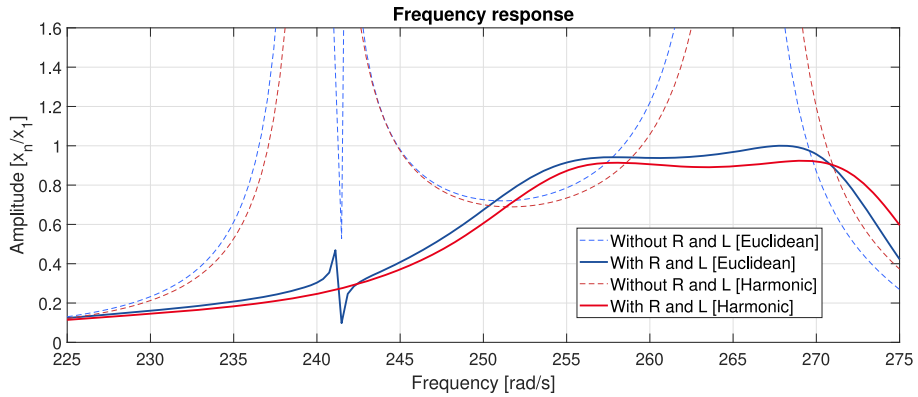

(a) Harmonic response for 1 pair of patches.

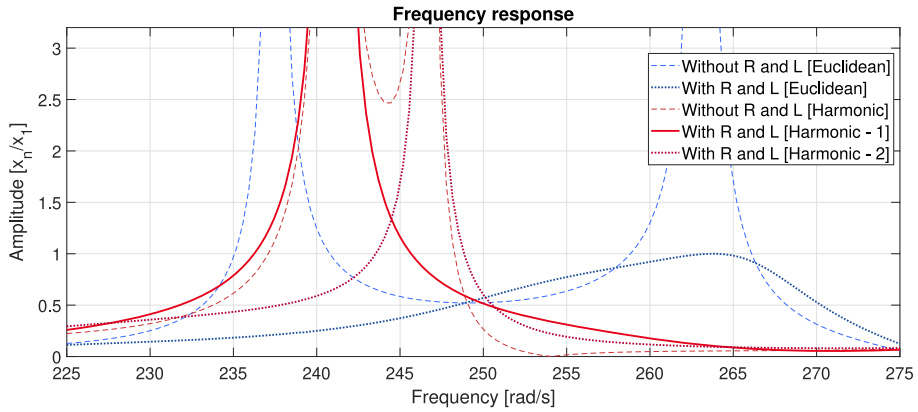

(b) Harmonic response for 4 pairs of patches.

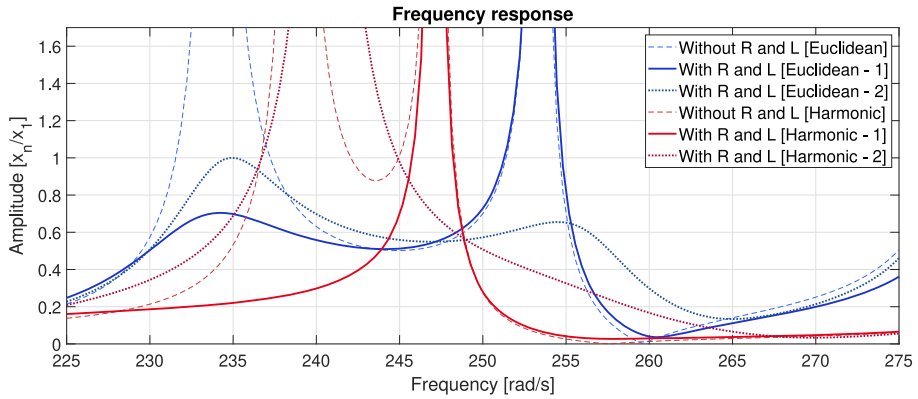

(c) Harmonic response for 9 pairs of patches.

Fig. 12 Individual harmonic analysis for different numbers of pairs of patches using Euclidean and Harmonic optimal points with different electrical connections, where label 1 do not consider the modal charge signal, while label 2 considers the modal charge signal of mode 8

Table 9 Local minimum computed by Maximum Harmonic Average for each number of pairs of patches

Pairs of patches	Position Values						Electrical Values		k_e^2
	x_1 [%]	x_2	x_3	y_1	y_2	y_3	L_p [H]	R_p [kΩ]	[%]
1	32	–	–	50	–	–	0.79	5.10	[1.2420, 1.5037, 1.4498]
4	60	66	–	49	100	–	0.82	5.37	[0.9346, 0.9100, 2.7827]
9	56	70	100	50	100	100	0.85	5.81	[1.1364, 0.7271, 1.9913]

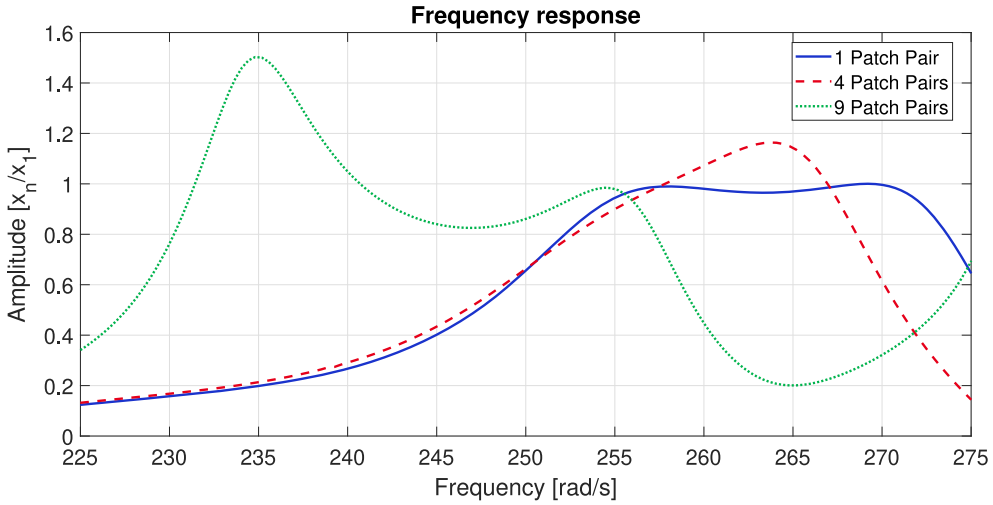

Fig. 13 Harmonic analysis of the frequency range encompassing modes 6, 7, and 8, utilizing the optimal configurations for each number of pairs of patches

As shown in Fig. 12, some graphs, such as 12b and 12c, display multiple lines representing different position configurations. This occurs because, when multiple patches are used, the electrical connections between them become an additional factor. Since the multi-objective study considers a multi-modal analysis, the charge distribution across patches can vary depending on the mode being excited. In a single-shunt approach, addressing these modal variations poses a challenge, as the same geometric configuration can yield different responses based on the applied electrical configuration.

For instance, in Fig. 12b, two distinct electrical connections were applied to the harmonic optimal position, identified as labels 1 and 2. Similarly, in Fig. 12c, two different electrical connections were applied to both the harmonic and Euclidean optimal positions, also marked with labels 1 and 2. These configurations focus on damping specific modes within the frequency range, as the single-shunt circuit cannot effectively address multiple modes simultaneously. Label 1 corresponds to configurations that disregard the influence of the modal charge signal that is, connecting the outer surfaces of the pairs of patches together and the inner surfaces in the same way. In contrast, label 2 accounts for the modal charge signal of mode 8, where pairs with negative modal charges are connected alternately.

Accordingly, by comparing the optimal results for each quantity of patches illustrated in Fig. 12, specifically 1 pair of patch (Harmonic), 4 pairs of patches (Euclidean), and 9 pairs of patches (Euclidean 2), it is possible to have the response showed by Fig. 13.

As illustrated in Fig. 13, the configuration with a single pair of patch exhibited the most effective damping at the resonance peak. This solution may be beneficial in cases involving multiple modes, as previously discussed, mainly, because, when the excited mode changes, configurations with more than one pair of patch needs to deal with issues due to the single-shunt implementation. However, the configuration with 4 patches also demonstrated satisfactory performance, while it exhibited a slightly higher peak, this peak occurred over a reduced frequency range in comparison with the single pair of patch case. Finally, nine pairs of patches configuration presented the most significant challenges with the single shunt electrical configuration. As can be seen, the implemented electrical configuration led to the reduction of the frequency range of mode 8, rather than modes 6 and 7, due to this, it has worse results in the initial frequencies. Consequently, this setup may

yield superior results with a multi-shunt configuration, where each patch operates within its own electrical circuit, thereby eliminating the issues caused by shared connections.

7 Conclusions

This article addressed the optimal patch positions for various configurations in a plate structure, considering both individual and multiple vibration modes. Furthermore, electrical components were connected to the patches, already in their ideal positions, to validate their impact on the damping effect. These analyses were performed using finite element simulations. Using input parameters specifying patch locations on the plate, the software calculated the natural frequencies in both open-circuit and short-circuit configurations, allowing for the estimation of the EMCC. The GLODS and DMS optimization algorithms were then used to determine the optimal patch positions that yielded the maximum EMCC values when studied both individual or multiple modes.

Additionally, the analysis of different patch configurations allowed for a comparison between the use of multiple pairs of patches versus a single one. It was observed that, for most vibration modes, the EMCC values for a single pair were higher. This is primarily because the optimal positions often place patches close together, and as the number of pairs of patches increases, the minimum distance between them decreases, which leads to a reduction in EMCC. However, while the single pair of patch provided higher EMCC values, the differences compared to the multiple pairs configurations were relatively small.

When analyzing a broader frequency range that encompasses multiple modes, the multi-pairs approach may offer better performance. This is because a larger number of pairs of patches can be strategically positioned based on the specific modes being studied. Nevertheless, as demonstrated in this paper, despite the potential advantages of the multiple pairs of patches approach, the single pair still resulted in better damping of resonance peaks. This is due to the limitations imposed by the single-shunt connection in the multi-pairs configuration.

In conclusion of the multi-objective analysis, while the single pair of patch configuration provided superior damping performance, the difference was minimal compared to the four pairs of patches case. The nine pairs configuration also faced challenges, primarily due to the electrical connections between patches. Future studies should explore the use of a multi-shunt approach, where each pair of patch operates within its own circuit, potentially improving damping performance by eliminating the issues caused by shared electrical connections in case of multi-modes.

Acknowledgements The authors acknowledge Fundação para a Ciência e a Tecnologia for its financial support via the project LAETA Base Funding (https://doi.org/10.54499/UIDB/50022/2020) and LAETA Programmatic Funding (https://doi.org/10.54499/UIDP/50022/2020).

Funding Open access funding provided by FCT|FCCN (b-on).

Declarations

Conflict of interest The authors have no relevant financial or non-financial interests to disclose.

References

1. Chopra, I.: Review of state of art of smart structures and integrated systems. AIAA journal **40**(11), 2145–2187 (2002)
2. Bendine, K., Boukhoulda, F., Haddag, B., Nouari, M.: Active vibration control of composite plate with optimal placement of piezoelectric patches. Mechanics of Advanced Materials and Structures **26**(4), 341–349 (2019)
3. Forward, R.L.: Electronic damping of vibrations in optical structures. Applied optics **18**(5), 690–697 (1979)
4. Hagood, N.W., Von Flotow, A.: Damping of structural vibrations with piezoelectric materials and passive electrical networks. Journal of sound and vibration **146**(2), 243–268 (1991)
5. Araújo, A., Madeira, J.: Multiobjective optimization solutions for noise reduction in composite sandwich panels using active control. Composite Structures **247**, 112440 (2020)

6. Agnes, G.S.: Development of a modal model for simultaneous active and passive piezoelectric vibration suppression. Journal of Intelligent Material Systems and Structures **6**(4), 482–487 (1995)
7. Tang, J., Wang, K.-W.: Active-passive hybrid piezoelectric networks for vibration control: comparisons and improvement. Smart Materials and Structures **10**(4), 794 (2001)
8. Agnes, G.S.: Active/passive piezoelectric vibration suppression. In: Smart Structures and Materials 1994: Passive Damping, **2193**, pp. 24–34 (1994). SPIE
9. Trindade, M.A., Benjeddou, A.: Hybrid active-passive damping treatments using viscoelastic and piezoelectric materials: review and assessment. Journal of Vibration and Control **8**(6), 699–745 (2002)
10. Wu, S.-y.: Piezoelectric shunts with a parallel rl circuit for structural damping and vibration control. In: Smart Structures and Materials 1996: Passive Damping and Isolation, vol. 2720, pp. 259–269 (1996). Spie
11. Krenk, S., Høgsberg, J.: Tuned resonant mass or inerter-based absorbers: unified calibration with quasi-dynamic flexibility and inertia correction. Proceedings of the Royal Society A: Mathematical, Physical and Engineering Sciences **472**(2185), 20150718 (2016)
12. Høgsberg, J., Krenk, S.: Calibration of piezoelectric rl shunts with explicit residual mode correction. Journal of Sound and Vibration **386**, 65–81 (2017)
13. Toftekær, J.F., Benjeddou, A., Høgsberg, J.: New piezoelectric shunt tuning method based on the effective electromechanical coupling coefficient: validation and 3d implementation. 7th International Symposium on Aircraft Materials (2018)
14. Toftekær, J.F., Benjeddou, A., Høgsberg, J.: General numerical implementation of a new piezoelectric shunt tuning method based on the effective electromechanical coupling coefficient. Mechanics of Advanced Materials and Structures **27**(22), 1908–1922 (2020)
15. Trindade, M.A., Benjeddou, A.: Effective electromechanical coupling coefficients of piezoelectric adaptive structures: critical evaluation and optimization. Mechanics of Advanced Materials and Structures **16**(3), 210–223 (2009)
16. Davis, C., Lesieutre, G.A.: A modal strain energy approach to the prediction of resistively shunted piezoceramic damping. Journal of Sound and Vibration **184**(1), 129–139 (1995)
17. Anton, S.R., Sodano, H.A.: A review of power harvesting using piezoelectric materials (2003–2006). Smart materials and Structures **16**(3), 1 (2007)
18. Beeby, S.P., Tudor, M.J., White, N.: Energy harvesting vibration sources for microsystems applications. Measurement science and technology **17**(12), 175 (2006)
19. Al-Ajmi, M., Benjeddou, A.: Damage indication in smart structures using modal effective electromechanical coupling coefficients. Smart materials and structures **17**(3), 035023 (2008)
20. Ducarne, J., Thomas, O., Deü, J.-F.: Placement and dimension optimization of shunted piezoelectric patches for vibration reduction. Journal of Sound and Vibration **331**(14), 3286–3303 (2012)
21. Bachmann, F., Bergamini, A.E., Ermanni, P.: Optimum piezoelectric patch positioning: A strain energy-based finite element approach. Journal of intelligent material systems and structures **23**(14), 1575–1591 (2012)
22. Cotrim, B.R., Araújo, A.L., Madeira, J.F.: Optimal resistive shunted damping configurations for multi-modal noise reduction in sandwich panels. Acta Mechanica **234**(1), 221–237 (2023)
23. Araújo, A.L., Aguilar Madeira, J.F.: Optimal passive shunted damping configurations for noise reduction in sandwich panels. Journal of Vibration and Control **26**(13–14), 1110–1118 (2020)
24. ANSYS, Inc.: ANSYS 18.0 Documentation. Canonsburg, Pennsylvania, USA (2017). ANSYS, Inc
25. Custódio, A.L., Madeira, J.A.: Glods: global and local optimization using direct search. Journal of global optimization **62**, 1–28 (2015)
26. Custódio, A.L., Madeira, J.A., Vaz, A.I.F., Vicente, L.N.: Direct multisearch for multiobjective optimization. SIAM Journal on Optimization **21**(3), 1109–1140 (2011)
27. Correia, V.M.F., Madeira, J.A., Araújo, A.L., Soares, C.M.M.: Multiobjective optimization of ceramic-metal functionally graded plates using a higher order model. Composite Structures **183**, 146–160 (2018)
28. Portal: Lead zirconate titanate (PZT-5H). https://www.efunda.com/materials/piezo/material_data/matdata_output.cfm?Material_ID=PZT-5H. Last accessed: 2024-07-03 (2024)